REPORT

PLANT SCIENCE

TIR domains of plant immune receptors are NAD$^+$-cleaving enzymes that promote cell death

Li Wan[1]*, Kow Essuman[2]*, Ryan G. Anderson[1], Yo Sasaki[2], Freddy Monteiro[1,3], Eui-Hwan Chung[1], Erin Osborne Nishimura[4], Aaron DiAntonio[5,6], Jeffrey Milbrandt[2,6,7]†, Jeffery L. Dangl[1]†, Marc T. Nishimura[8]†

Plant nucleotide-binding leucine-rich repeat (NLR) immune receptors activate cell death and confer disease resistance by unknown mechanisms. We demonstrate that plant Toll/interleukin-1 receptor (TIR) domains of NLRs are enzymes capable of degrading nicotinamide adenine dinucleotide in its oxidized form (NAD$^+$). Both cell death induction and NAD$^+$ cleavage activity of plant TIR domains require known self-association interfaces and a putative catalytic glutamic acid that is conserved in both bacterial TIR NAD$^+$-cleaving enzymes (NADases) and the mammalian SARM1 (sterile alpha and TIR motif containing 1) NADase. We identify a variant of cyclic adenosine diphosphate ribose as a biomarker of TIR enzymatic activity. TIR enzymatic activity is induced by pathogen recognition and functions upstream of the genes *enhanced disease susceptibility 1* (*EDS1*) and *N requirement gene 1* (*NRG1*), which encode regulators required for TIR immune function. Thus, plant TIR-NLR receptors require NADase function to transduce recognition of pathogens into a cell death response.

Plants rely on an innate immune system to detect potential pathogens. Molecular identification of disease resistance genes has revealed that resistance to pathogens from all kingdoms is conferred by nucleotide-binding leucine-rich repeat (NLR) immune receptors (*1*). Despite their agronomic value and over 25 years of molecular study, mechanistic explanations for how NLR receptors trigger cell death and disease resistance remain opaque (*2*, *3*).

Toll/interleukin-1 receptor (TIR) domains are found in both intracellular plant TIR-NLR receptors and the animal cell surface Toll-like receptor system (*3*). The noncanonical animal TIR protein SARM1 (sterile alpha and TIR motif containing 1) is required for Wallerian degeneration in axons after nerve injury (*4*, *5*). Although other animal TIRs function as oligomeric signaling scaffolds, SARM1 has a distinct mechanism: SARM1's TIR domain is the founding member of a class of enzymes that cleave nicotinamide adenine dinucleotide (oxidized form; NAD$^+$) (fig. S1) (*6*). SARM1-triggered cell death is proposed to result from severe depletion of NAD$^+$ (*4*, *6*). Prokaryotic TIR domains also metabolize NAD$^+$ and NADP$^+$ (*7*). NAD$^+$ and NADP$^+$ are essential metabolic components, and their cleavage is implicated in diverse interspecies interactions, including toxin-triggered cell death (*8*), effector-mediated immunosuppression (*9*), antiphage defenses (*10*), and bacterial competition (*11*).

Plant TIR-NLRs typically trigger hypersensitive cell death in response to pathogens. There is no evidence that plant TIRs function as scaffolds, as canonical animal TIRs do, and transient expression of some plant TIRs is sufficient to cause ectopic cell death. We sought to determine if plant TIR domains are mechanistically similar to SARM1. A structural homology search with SARM1-TIR returned plant TIR domains with high confidence (table S1). Homology models suggest that SARM1's putative catalytic glutamic acid at position 642 (E642) (*6*) and neighboring residues are positionally conserved in plants (Fig. 1A). Of 146 *Arabidopsis* TIR domains from the reference genome, 131 contain this conserved glutamic acid (Fig. 1B and table S2). TIR domains lacking the glutamic acid have genomic signatures reminiscent of the cell death–inactive "sensor" NLR RRS1 (table S2 and fig. S2) (*12*, *13*). Thus, the putative catalytic residue of SARM1 is present in potentially active plant TIR domains but absent from TIR-NLRs likely to lack autonomous activity.

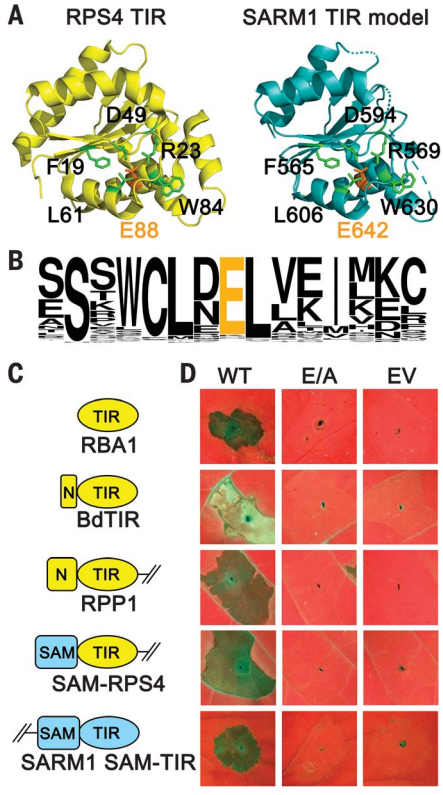

Fig. 1. Plant TIR proteins require a conserved putative catalytic residue for cell death activity in planta. (**A**) A homology model of SARM1-TIR (right, blue) indicates that its putative catalytic residue (E642, orange) is positioned similarly to E88 in the plant TIR RPS4 (PDB 4C6R; left, yellow). Neighboring conserved residues are green (with black labels). (**B**) Sequence pileup of the 146 TIR domains from the *Arabidopsis* Col-0 genome. (**C**) Proteins expressed in planta. Plant TIR proteins are shown in yellow, and human SARM1 domains are shown in blue. The NBS-LRR autoinhibitory domains are deleted in the RPP1$_{NdA}$ and RPS4 truncations. N, N-terminal extension; SAM, oligomerization domain from human SARM1. (**D**) In planta phenotypes of TIR proteins. RBA1 and autoactive SARM1 were expressed in *Nicotiana benthamiana*, and other TIRs were expressed in *Nicotiana tabacum*. Putative catalytic mutants (E/A) lose autoactive cell death capabilities. WT, wild type; EV, empty vector. Full images and protein accumulation data are shown in fig. S3.

To determine if the putative catalytic residue is functionally required, we generated glutamic acid–to–alanine mutations in the *Arabidopsis* TIR-only immune receptor RBA1 and the TIR domains of the *Arabidopsis* TIR-NLR immune receptors RPS4 and RPP1$_{NdA}$ (*13*–*15*). We also tested a TIR-only protein (BdTIR) of unknown

[1]Department of Biology and Howard Hughes Medical Institute, University of North Carolina, Chapel Hill, NC 27599, USA. [2]Department of Genetics, Washington University School of Medicine, St. Louis, MO 63110, USA. [3]Center for Research in Agricultural Genomics (CRAG), CSIC-IRTA-UAB-UB, 08193 Barcelona, Spain. [4]Department of Biochemistry and Molecular Biology, Colorado State University, Fort Collins, CO 80523, USA. [5]Department of Developmental Biology, Washington University School of Medicine, St. Louis, MO 63110, USA. [6]Needleman Center for Neurometabolism and Axonal Therapeutics, Washington University School of Medicine, St. Louis, MO 63110, USA. [7]McDonnell Genome Institute, Washington University School of Medicine, St. Louis, MO 63108, USA. [8]Department of Biology, Colorado State University, Fort Collins, CO 80523, USA.
*These authors contributed equally to this work.
†Corresponding author. Email: marcusn@colostate.edu (M.T. N.); jdangl@email.unc.edu (J.L.D.); jmilbrandt@wustl.edu (J.M.)

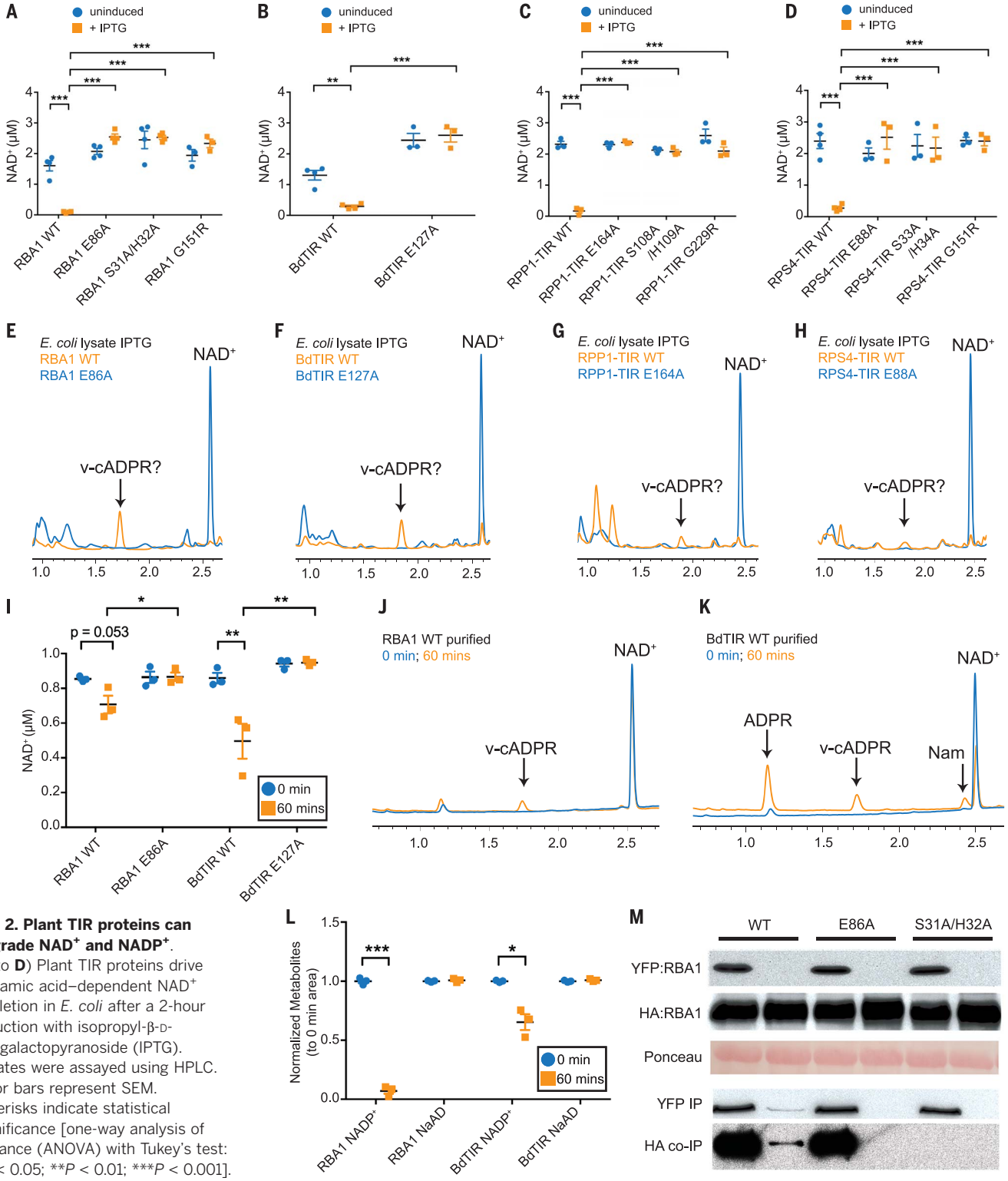

Fig. 2. Plant TIR proteins can degrade NAD$^+$ and NADP$^+$. (**A** to **D**) Plant TIR proteins drive glutamic acid–dependent NAD$^+$ depletion in *E. coli* after a 2-hour induction with isopropyl-β-D-thiogalactopyranoside (IPTG). Lysates were assayed using HPLC. Error bars represent SEM. Asterisks indicate statistical significance [one-way analysis of variance (ANOVA) with Tukey's test: *P < 0.05; **P < 0.01; ***P < 0.001]. (**E** to **H**) HPLC results with *E. coli* lysates [from assays shown in (A) to (D)]. (**I**) In vitro transcription-translation–generated TIR-only proteins lowered NAD$^+$ levels relative to putative catalytic mutants. Statistical significance levels, calculated separately for each gene and indicated by asterisks, are the same as for (A) to (D). (**J**) HPLC traces corresponding to (I) indicate RBA1-generated v-cADPR. (**K**) HPLC traces corresponding to (I) show that BdTIR decreases NAD$^+$ and leads to accumulation of nicotinamide, ADPR, and v-cADPR. (**L**) Plant TIR-only proteins generated by in vitro transcription-translation degrade NADP$^+$, but not the related molecule NaAD, after 60 min. Error bars represent SEM. Statistical significance was assessed using Welch's t test: *P < 0.05; ***P < 0.001. (**M**) Mutation of RBA1's putative catalytic residue (E86A) does not affect coimmunoprecipitation (co-IP) of hemagglutinin-tagged RBA1 (HA:RBA1) with yellow fluorescent protein-tagged RBA1 (YFP:RBA1) from *N. benthamiana*. WT, wild type. Amino acid abbreviations: A, alanine; E, glutamic acid; G, glycine; H, histidine; R, arginine; S, serine. The mutant protein E86A indicates a change at residue 86 from glutamic acid to alanine; the same nomenclature is used for other mutant proteins.

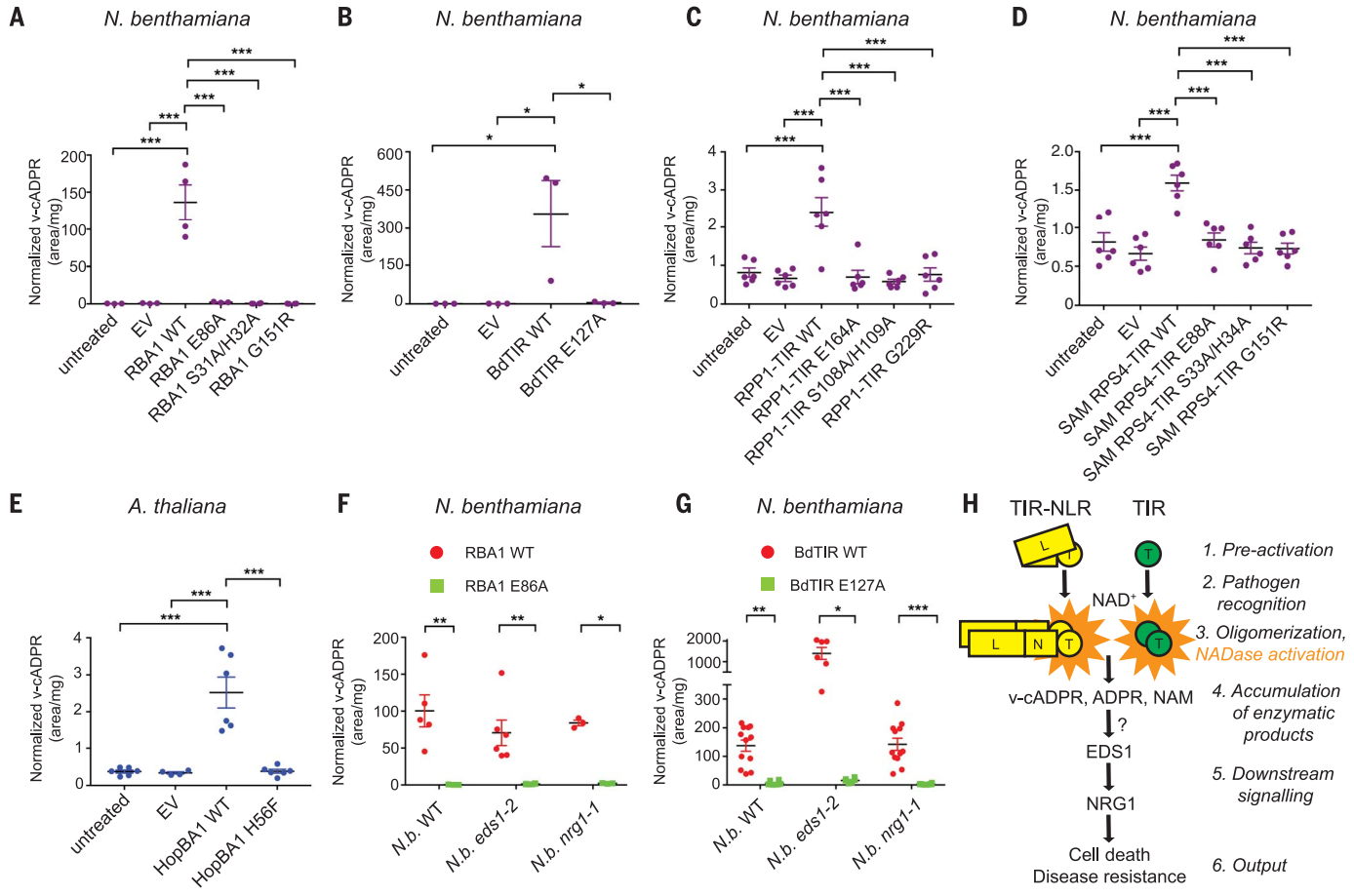

Fig. 3. TIRs produce v-cADPR in planta. (**A** to **D**) v-cADPR accumulates after transient expression of plant TIRs. v-cADPR does not accumulate in plants expressing empty vector (EV) or TIR loss-of-function mutants. Experiments shown in (C) and (D) were performed together and share untreated and EV data. Error bars represent SEM. Asterisks indicate statistical significance (one-way ANOVA with Tukey's test: $*P < 0.05$; $***P < 0.001$). (**E**) v-cADPR accumulates in *Arabidopsis* (Ag-0) 24 hours after inoculation with *P. fluorescens* (HopBA1). $HopBA1_{H56F}$ is encoded by a loss-of-function mutant [with histidine (H) at residue 56 changed to phenylalanine (F)] (*14*). (**F** and **G**) v-cADPR accumulates upon RBA1 and BdTIR expression in *N. benthamiana* and *eds1-2* and *nrg1-1* mutants. Error bars represent SEM. Asterisks indicate statistical significance [one-way ANOVA with Tukey's test for (F) and Kruskal-Wallis with Dunn's test for (G): $*P < 0.05$; $**P < 0.01$; $***P < 0.001$]. (**H**) Hypothetical pathway wherein TIR enzymatic function is induced by effector recognition and activation by TIR-NLR (left) or by TIR only (right). This leads to accumulation of signaling products derived from NAD^+ that accumulate upstream of EDS1/NRG1. T, TIR; N, NBD; L, LRR. Definitions of amino acid abbreviations and mutation designations are provided in the Fig. 2 legend.

function from the monocot *Brachypodium distachyon*. Monocot genomes have no full-length TNL immune receptors (*16*). All four TIRs triggered glutamic acid–dependent cell death in *Nicotiana* species (Fig. 1, C and D). In our study, the RPS4 TIR required fusion to an orthologous oligomerization domain [the sterile alpha motif (SAM) domain of SARM1] to trigger cell death (Fig. 1, C and D, and fig. S4). Consistent with our transient-expression assay results, mutants disrupting the conserved glutamic acid were identified in genetic screens as suppressors of TIR and TIR-NLR function (table S3). Expression of an autoactive fragment of SARM1 also triggered glutamic acid–dependent cell death in planta (Fig. 1C). Thus, the putative SARM1 catalytic residue is conserved and functionally required in plant TIRs.

Similar to SARM1-TIR (*6*, *7*), expression of plant TIR domains in *Escherichia coli* resulted in strong NAD^+ depletion, as measured by high-performance liquid chromatography (HPLC) (Fig. 2, A to D, and fig. S5). As with SARM1 (*6*, *7*), activity was dependent on the conserved glutamic acid (Fig. 2, A to D, and fig. S5). We observed accumulation of potential breakdown products accompanying NAD^+ depletion (Fig. 2, E to H). To characterize reaction products and demonstrate the intrinsic enzymatic activity of plant TIR domains, we purified RBA1 and BdTIR after in vitro transcription-translation and tested their ability to degrade NAD^+. Both HPLC and mass spectrometry analysis revealed that, like SARM1-TIR, purified RBA1 and BdTIR proteins degrade NAD^+ into nicotinamide (Fig. 2, I to K, and fig. S6, A and B). Purified BdTIR additionally produced adenosine diphosphate ribose (ADP-ribose) from the NAD^+ cleavage reaction (Fig. 2K and fig. S6C). The NAD^+ cleavage activity of RBA1 and BdTIR was dependent on the putative catalytic glutamic acid residue (Fig. 2I). Unlike SARM1, plant TIRs also generated an NAD^+ cleavage product that appears identical to an NAD^+ cleavage product from the archaeal TIR protein TcpO (fig. S7) (*7*). This product, which derives from the same parent ion as cyclic ADP-ribose (cADPR) but has a distinct chromatography retention time, is suggestive of a cyclization variant of cADPR, termed v-cADPR (*7*). v-cADPR serves as a proxy for plant TIR NAD cleavage (NADase) activity, as its accumulation is dependent on the putative catalytic glutamic acid (Fig. 2, E to H). SARM1-TIR cleaves NAD^+ in vitro to produce cADPR rather than v-cADPR (fig. S5F) (*6*) and appears to have higher activity than plant TIRs in this assay (fig. S5, E and G, and Fig. 2I), indicating mechanistic differences. We observed NAD^+ depletion by RPS4 and RPP1 TIR domains in the *E. coli* assay but were unable to confirm NAD^+-cleaving enzyme (NADase)

activity with these TIR domains as in vitro–purified proteins. We speculate that this assay fails to recreate functionally relevant higher-order structures that are generated during expression in *E. coli*. SARM1-TIR can degrade $NADP^+$ but not another NAD^+-related molecule, nicotinic acid adenine dinucleotide (NaAD) (*7*). Similar to SARM1-TIR, RBA1 and BdTIR proteins degraded $NADP^+$ (Fig. 2L) into nicotinamide and ADP-ribose phosphate (fig. S6, D to G) but did not degrade NaAD (Fig. 2L and fig. S1). Altogether, these results support our hypothesis that plant TIR domains are enzymes.

Plant TIR domains require two self-association interfaces for immune function (fig. S8) (*3*). To determine if self-association is required for NADase activity, we generated TIR domains containing demonstrated, or proposed, loss-of-self–association mutations (*13*, *14*). Mutation of either AE- or DE-type self-association interfaces abolished TIR cell death in planta (figs. S3, S4, and S8B) and NADase activity in *E. coli* (Fig. 2, A, C, and D). The in planta self-association requirements were retained in the human HsSAM-RPS4 TIR fusion (fig. S4, C and D), despite fusion to the SAM oligomerization domain, demonstrating that specific TIR-TIR interaction is required for function. We asked if mutation of the putative catalytic residue had an impact on self-association as measured by coimmunoprecipitation. $RBA1_{SH/AA}$ lost self-association (Fig. 2M) (*14*), but the putative catalytically dead $RBA1_{E86A}$ mutant retained self-association (Fig. 2M). This result is consistent with the hypothesis that TIR enzymatic activity is downstream of, and promoted by, self-association, thus explaining why plant TIR self-association is a common requirement for function.

Activation of SARM1 in neurons leads to strong NAD^+ depletion and subsequent axonal demise (*4*). In planta, the autoactive SARM1 truncation strongly depletes NAD^+ (fig. S9A). Consistent with an apparent weaker activity of plant TIRs in vitro, we have been unable to detect depletion of NAD^+ after transient expression of TIRs in planta (fig. S9, A to C). As noted above (Fig. 2), NAD^+ cleavage by plant TIR domains was accompanied by production of nicotinamide, ADPR, and v-cADPR. NAD^+ cleavage is thus a plausible signaling event, as ADPR and cADPR trigger calcium influx to the cytoplasm (*17*, *18*), and this is correlated with plant NLR function (*19*).

To validate that plant TIRs are indeed NADases in planta, we measured TIR-dependent accumulation of v-cADPR in planta. v-cADPR accumulated in planta in response to plant TIR transient expression (Fig. 3, A to D). Similar to our *E. coli* assay (Fig. 2, E to H), the levels of v-cADPR produced in planta by the TIR-NLR TIRs were lower than those induced by the TIR-only proteins. TIR-dependent accumulation of v-cADPR in planta was dependent upon the putative catalytic glutamic acid (Fig. 3, A to D) and on self-association (Fig. 3, A, C, and D). We measured v-cAPDR accumulation in a biologically relevant system. Delivery of the type III effector HopBA1 by *Pseudomonas fluorescens* activates RBA1-dependent cell death in *Arabidopsis* (*14*). HopBA1 induced v-cAPDR accumulation in *Arabidopsis*, whereas bacteria containing a loss-of-function allele, $HopBA1_{H56F}$ (*14*), did not (Fig. 3E). Cell death triggered by non-TIR immune function did not induce v-cADPR accumulation (fig. S9, E and F). In summary, v-cADPR is an in planta biomarker of plant TIR enzymatic function. The lack of in planta NAD^+ depletion by plant TIRs suggests that plant TIRs function through an NADase-dependent signaling mechanism distinct from that for animal SARM1 NAD^+ depletion.

All tested TIR-NLR phenotypes require the catalytically inactive lipase ENHANCED DISEASE SUSCEPTIBILITY 1 (EDS1) (*20*, *21*). Consistent with this requirement, autoactivity triggered by the four tested plant TIR domains was EDS1 dependent (fig. S10). In contrast, autoactive SARM1 cell death in planta was EDS1 independent (fig. S10), again suggesting that plant and animal TIR NADases act via different mechanisms to drive cell death. The functional mechanism of EDS1 is unknown, but this lipase can be found in complex with TIR-NLR proteins (*22*). Thus, EDS1 could be required for TIR function directly or be required for downstream signaling. Similarly, protein encoded by *N-required gene 1* (*NRG1*), a coiled-coil "helper" NLR, functions downstream of EDS1 (*23*). v-cADPR accumulates in both *eds1* and *nrg1* mutants upon expression of RBA1 or BdTIR, despite a lack of cell death (Fig. 3, F and G, and fig. S11). Thus, TIR enzymatic activity, via the generation of metabolites such as v-cADPR, may signal downstream through EDS1 and then NRG1 to promote cell death (Fig. 3H).

NAD^+ is a signaling substrate that influences myriad aspects of biology, including DNA repair, aging, and transcriptional regulation, in addition to its metabolic function (*24*). Our results establish plant TIR domains as enzymes that can cleave NAD^+ and $NADP^+$. Direct cell death by NAD^+ depletion would not require downstream genetic components, suggesting that SARM1 and plant TIRs trigger cell death by distinct mechanisms and that the latter generate a signal via NADase activity that activates EDS1 and NRG1. Our data present a framework for understanding plant TIRs as enzymes that cleave NAD^+ to activate immunity.

REFERENCES AND NOTES

1. J. D. G. Jones, J. L. Dangl, *Nature* **444**, 323–329 (2006).
2. J. D. G. Jones, R. E. Vance, J. L. Dangl, *Science* **354**, aaf6395 (2016).
3. X. Zhang, P. N. Dodds, M. Bernoux, *Annu. Rev. Phytopathol.* **55**, 205–229 (2017).
4. J. Gerdts, E. J. Brace, Y. Sasaki, A. DiAntonio, J. Milbrandt, *Science* **348**, 453–457 (2015).
5. J. Gerdts, D. W. Summers, Y. Sasaki, A. DiAntonio, J. Milbrandt, *J. Neurosci.* **33**, 13569–13580 (2013).
6. K. Essuman *et al.*, *Neuron* **93**, 1334–1343.e5 (2017).
7. K. Essuman *et al.*, *Curr. Biol.* **28**, 421–430.e4 (2018).
8. D. Pajuelo *et al.*, *Cell Rep.* **24**, 429–440 (2018).
9. T. Shidore *et al.*, *PLOS Pathog.* **13**, e1006442 (2017).
10. S. Doron *et al.*, *Science* **359**, eaar4120 (2018).
11. J. Y. Tang, N. P. Bullen, S. Ahmad, J. C. Whitney, *J. Biol. Chem.* **293**, 1504–1514 (2018).
12. M. Narusaka *et al.*, *Plant J.* **60**, 218–226 (2009).
13. S. J. Williams *et al.*, *Science* **344**, 299–303 (2014).
14. M. T. Nishimura *et al.*, *Proc. Natl. Acad. Sci. U.S.A.* **114**, E2053–E2062 (2017).
15. K. J. Schreiber, A. Bentham, S. J. Williams, B. Kobe, B. J. Staskawicz, *PLOS Pathog.* **12**, e1005769 (2016).
16. Z. Q. Shao *et al.*, *Plant Physiol.* **170**, 2095–2109 (2016).
17. R. Fliegert, A. Gasser, A. H. Guse, *Biochem. Soc. Trans.* **35**, 109–114 (2007).
18. Y. Wu *et al.*, *Science* **278**, 2126–2130 (1997).
19. M. Grant *et al.*, *Plant J.* **23**, 441–450 (2000).
20. N. Aarts *et al.*, *Proc. Natl. Acad. Sci. U.S.A.* **95**, 10306–10311 (1998).
21. S. Wagner *et al.*, *Cell Host Microbe* **14**, 619–630 (2013).
22. S. U. Huh *et al.*, *PLOS Pathog.* **13**, e1006376 (2017).
23. T. Qi *et al.*, *Proc. Natl. Acad. Sci. U.S.A.* **115**, E10979–E10987 (2018).
24. T. G. Demarest *et al.*, *Annu. Rev. Cancer Biol.* **3**, 105–130 (2019).

ACKNOWLEDGMENTS

We thank S. Grant and M. Redinbo for careful reading and discussion of the manuscript. We thank B. Staskawicz for sharing *N. benthamiana eds1* and *nrg1* mutants. We thank B. Kobe for sharing the sequence of the SARM1 SAM domain pentamutant. We thank K. Simburger and T. Fahrner for technical assistance. We thank C. Argueso and D. Bush for use of facilities. We thank B. Staskawicz, K. H. Sohn, and F. El Kasmi for plasmids. **Funding:** This work was supported by the National Science Foundation (grant IOS-1758400 to J.L.D. and M.T.N.) and National Institutes of Health (grants GM107444 to J.L.D., RF1AG013730 to J.M., and R01NS087632 to J.M. and A.D.). J.L.D. is a Howard Hughes Medical Institute (HHMI) Investigator. M.T.N. was supported by startup funds from Colorado State University. R.G.A. was supported by an NIH Ruth L. Kirschstein NRSA fellowship (F32GM108226). K.E. was an HHMI Medical Research Fellow. F.M. is supported by a grant from the Gordon and Betty Moore Foundation (GBMF4725) to the Two Blades Foundation. **Author contributions:** L.W., K.E., R.G.A., J.M., J.L.D., and M.T.N. conceived and designed the study. L.W., K.E., R.G.A., Y.S., F.M., E.C., and M.T.N. generated data. L.W., K.E., J.M., J.L.D., and M.T.N. wrote the initial manuscript. All authors edited the final version of the manuscript. **Competing interests:** J.M. and Y.S. may derive income from licensing technology to ChromaDex. J.M. and A.D. are cofounders and scientific advisors of Disarm Therapeutics. K.E., Y.S., A.D., and J.M. may derive income from licensing of technology to Disarm Therapeutics. **Data and materials availability:** All data are available in the manuscript or the supplementary materials.

SUPPLEMENTARY MATERIALS

science.sciencemag.org/content/365/6455/799/suppl/DC1
Materials and Methods
Figs. S1 to S11
Tables S1 to S3
References
Data S1 to S3

28 February 2019; accepted 10 July 2019
10.1126/science.aax1771

TIR domains of plant immune receptors are NAD$^+$-cleaving enzymes that promote cell death

Li Wan, Kow Essuman, Ryan G. Anderson, Yo Sasaki, Freddy Monteiro, Eui-Hwan Chung, Erin Osborne Nishimura, Aaron DiAntonio, Jeffrey Milbrandt, Jeffery L. Dangl and Marc T. Nishimura

Science **365** (6455), 799-803.
DOI: 10.1126/science.aax1771

NAD depletion as pathogen response

One way that plants respond to pathogen infection is by sacrificing the infected cells. The nucleotide-binding leucine-rich repeat immune receptors responsible for this hypersensitive response carry Toll/interleukin-1 receptor (TIR) domains. In two papers, Horsefield *et al.* and Wan *et al.* report that these TIR domains cleave the metabolic cofactor nicotinamide adenine dinucleotide (NAD $^+$) as part of their cell-death signaling in response to pathogens. Similar signaling links mammalian TIR-containing proteins to NAD $^+$ depletion during Wallerian degeneration of neurons.

Science, this issue p. 793, p. 799

Supplementary Materials for

TIR domains of plant immune receptors are NAD$^+$-cleaving enzymes that promote cell death

Li Wan*, Kow Essuman*, Ryan G. Anderson, Yo Sasaki, Freddy Monteiro, Eui-Hwan Chung, Erin Osborne Nishimura, Aaron DiAntonio, Jeffrey Milbrandt†, Jeffery L. Dangl†, Marc T. Nishimura†

*These authors contributed equally to this work.
†Corresponding author. Email: marcusn@colostate.edu (M.T.N.); jdangl@email.unc.edu (J.L.D.); jmilbrandt@wustl.edu (J.M.)

Published 23 August 2019, *Science* **365**, 799 (2019)
DOI: 10.1126/science.aax1771

This PDF file includes:

Other Supplementary Material for this manuscript includes the following:
(available at science.sciencemag.org/content/365/6455/799/suppl/DC1)

Data S1 to S3 (.xlsx and .doc)

Materials and Methods

Plant materials, growth conditions, extract preparation for metabolite identification.

Nicotiana benthamiana and *Nicotiana tabacum* were grown in walk-in growth rooms maintained at 24 °C/20 °C with a 16-h/8-h (day/night) cycle. In *Agrobacterium*-mediated transient expressions, relevant strains were grown overnight, and the cell pellet was resuspended in induction buffer containing 10 mM MES (pH 5.6), 10 mM $MgCl_2$, and 150 µM acetosyringone. *Agrobacteria* (GV3101 pMP90) were hand-injected with 1mL needleless syringes at OD_{600nm} of 0.8 (Injections into *N. benthamiana* included 0.1 OD_{600nm} of GV3101 carrying 35S:P19, a viral suppressor of gene silencing) into 5- to 6-week-old *N. benthamiana* or *N. tabacum* leaves. Images of cell-death phenotypes were taken 2-5 days post inoculation. For western blots to check protein expression of TIR domains, leaf samples of SARM1, RBA1 and MLA10 CC were collected at 26h post infiltration, while leave samples of BdTIR, SAM-RPS4 and RPP1 were collected 40h post infiltration. For NADase metabolite assays, leaf samples were collected at 26h post infiltration or 40h post infiltration, as above. Nine leaf disks (8 mm in diameter) from at least 4 leaves from 4 different plants were pooled and weighed, and then homogenized into powder and dissolved in 450 µL 50% (v/v) methanol and stored at -80 °C. 150 µL of supernatant after centrifugation was analyzed by mass spectrometry (see below).

Arabidopsis thaliana Ag-0 and Col-0 plants were grown in walk-in rooms maintained at 21° C/18° C with a 9-h/15-h (day/night) cycle. In *Pseudomonas fluorescens* (Pf0-1) or *Pseudomonas syringae pv. tomato DC3000* (DC3000) mediated effector-delivery assays, Pf0-1 or DC3000 strains were grown overnight, washed once with 10 mM $MgCl_2$ and then diluted in 10 mM $MgCl_2$ to an OD_{600nm} of 0.2 (Pf0-1) and an OD_{600nm} of 0.1 (DC3000). These cultures were hand-injected with needleless syringes into 4- to 6-week old *Arabidopsis* rosette leaves around 10 AM. The cell death phenotypes were recorded 24h and 30h post inoculation. For western blots to check protein levels, leaf samples were collected 24h post inoculation. For NADase metabolite assays, leaf samples were collected at 24h post infiltration. For NADase metabolite assays, leave samples were collected at 24h post infiltration. Six leaf disks (8mm in diameter) from 6 leaves from 6 different plants were pooled and weighed, and then homogenized into powder and dissolved in 300 µL 50% (v/v) methanol and stored at -80 °C. 150 µL of supernatant after centrifugation was analyzed by mass spectrometry (see below).

LC-MS/MS metabolite measurement.

Plant extracts were prepared as indicated above. For LC-MS/MS analysis, metabolites were extracted in 50% methanol in water and deproteinized with chloroform, and the aqueous phase was lyophilized and stored at -80°C until LC-MS/MS analysis. For LC-MS/MS, the metabolite samples were reconstituted with 5 mM ammonium formate, centrifuged 12,000 x g for 10 min, and the cleared supernatant was applied to the LC-MS/MS for metabolite identification and quantification. Liquid chromatography was performed by HPLC system (1290; Agilent) with an Atlantis T3 (2.1 x 150 mm, 3 µm; Waters) column. Samples (10 µl) were injected at a flow rate of 0.15 ml/min with 5 mM ammonium formate for mobile phase A and 100% methanol for mobile phase B;

metabolites were eluted with gradients of 2–6 min, 0–20% B; 6-8 min, 20-50% B; 8 - 10 min 50% B; 10 - 15 min, 50 - 0% B; 15 - 24 min, 0% B. The metabolites were detected with a Triple Quad mass spectrometer (6460; Agilent) under positive ESI multiple reaction monitoring (MRM). Metabolites were quantified by using area under the curve determined by MassHunter quantitative analysis tool (Agilent) and the retention time for each compounds were determined with standard compounds including NAD^+, cADPR, ADPR, Nam, v-cADPR, ADPRP reconstituted in 5 mM ammonium formate. The following mass-to-charge (m/z) for parent and product ion was used for detection of metabolites on LC-MS/MS: NAD+ (664 > 542); ADPR (560 > 136); Nam (123 > 80); cADPR (542 > 428); v-cADPR (542 >136); ADPRP (640 > 136).

Bacterial strains and growth conditions.

E. coli Top10 and *Agrobacterium tumefaciens* strain GV3101/pMP90 were grown in LB medium at 37 °C and 28 °C, respectively. *Pseudomonas* strains were grown in King's B medium at 28 °C. The antibiotic concentrations (μg/mL) used for *E. coli* were ampicillin 100, kanamycin 30, gentamycin 25, and spectinomycin 50. The antibiotic concentrations (μg/mL) used for *Agrobacterium* were gentamycin 50, kanamycin 100, rifampicin 100, and spectinomycin 100. The antibiotic concentrations (μg/mL) used for *Pseudomonas* were tetracycline 50, kanamycin 30, and rifampicin 50.

Plasmids.

Bacterial expression plasmids were cloned in pET24a+ (RPP1) or pET30a+ (others). Recombinant plasmids include, SARM1 – StrepTag-SARM1-TIR-HisTag (TIR: 561-724); RBA1 – StrepTag-RBA1-HisTag (TIR: 1-191); Bd – StrepTag-Bd-HisTag (TIR: 1-224); RPS4 – StrepTag-RPS4-HisTag (TIR: 1-200); RPP1 – HisTag-RPP1-StrepTag (TIR: 1-254). Plant expression constructs were generated using Gateway-compatible vector systems. Entry clone were generated by BP clonase in pDONR207 or synthesized in pUC57-Kan (Genescript). Site-directed mutants were generated by PCR mutagenesis. Cloning primers are available upon request. Plant expression vectors are from the pGWB600 series. Plant expression clones for BdTIR (NCBI accession XM_003560026) and HsSARM1 SAM-TIR were codon-optimized for Arabidopsis and synthesized by GenScript. The N-terminal HA-SAM vector was constructed by cloning the SAM domain from HsSARM1 (1xHA tag-SARM1$_{478\text{-}578}$-GGGGS) into the XbaI site of pGWB602. The RPS4$_{\text{Ws 1-250}}$ entry clone was a gift from Kee Hoon Sohn. The RPP1$_{\text{NdA 1-254}}$ entry clone was a gift from Brian Staskawicz. The MLA10 CC domain (endpoints: 1-160) entry clone was a gift from Farid El-Kasmi. RBA1 is from Arabidopsis accession Ag-0 (*14*).

Coimmunoprecipitation and western blotting.

A combination of *Agrobacterium* strains containing relevant constructs were infiltrated into two separate halves of *N. benthamiana* leaves. The leaf samples were collected and flash frozen in liquid nitrogen 36 h post infiltration. Frozen leaf tissue was ground in a mortar and pestle with liquid nitrogen and resuspended in 2 mL of extraction buffer [50 mM HEPES (pH 7.5), 50 mM NaCl, 10 mM EDTA (pH 8.0), 0.2% Triton X-100, 5 mM DTT with 1× plant protease inhibitor mixture (Sigma-Aldrich)]. Soluble supernatants were obtained by centrifugation twice at 10,000 × g for 15 min at 4 °C. 50

µL of α-GFP conjugated magnetic beads (Miltenyi Biotec) was added to each sample and incubated for 2.5 h with constant rotation at 4 °C. Samples were captured using separation columns (Miltenyi Biotec) and were washed with washing buffer (extraction buffer with 0.1% Triton X-100 and 150 mM NaCl) three times. Bound proteins were eluted in 120 µL elution buffer [50 mM Tris·HCl (pH 6.8), 50 mM DTT, 1% SDS, 1 mM EDTA (pH 8.0), 0.005% bromophenol blue, and 10% glycerol]. Samples were resolved by electrophoresis on 12% SDS/PAGE gels and transferred to nitrocellulose membrane. The membrane was blocked for 30 mins in 5% milk dissolved in TBS-T (TBS with 1% Tween) and blotted with HRP-conjugated antibodies overnight at 4 °C in TBS with TBS-T. The following antibody concentrations were used: α-GFP, 1:5,000 (Santa Cruz Biotechnology); α-HA, 1:2,000 (Santa Cruz Biotechnology).

Endogenous NAD^+ measurements in *E. coli*.

Recombinant plasmids in either pET24a+ (RPP1) or pET30a+ (others) were transformed into Shuffle T7 Express Competent *E. coli* (New England BioLabs). Single colonies were grown overnight and the next day, cultures were diluted in LB media, grown at 30°C until they reached an absorbance (A_{600}) of approximately 0.4-0.8. 0.1 mM IPTG final concentration was added to induce protein expression. Cultures were harvested approximately 2 hours later, and then normalized to A_{600} of approximately 0.5 ± 0.05. 500 µl of culture suspension was then aliquoted, and centrifuged. The supernatant was decanted, the pellet washed with PBS, and centrifuged again. Metabolites from the bacterial pellet were extracted by adding 200 µL 0.5M Perchloric acid ($HClO_4$). Samples were then placed on ice for at least 10 minutes, spun down, and supernatant collected. 180 µL of supernatant was then added to approximately 67 µL of 3M Potassium Carbonate (K_2CO_3). Samples were placed on ice for at least 10 minutes, and centrifuged. NAD^+ metabolites were then measured by HPLC as described below.

HPLC metabolite measurement.

Potassium carbonate neutralized reactions were centrifuged, and the supernatant (90 µL) containing the extracted metabolites was mixed with 0.5M Potassium Phosphate buffer (10 µL). Metabolites were analyzed by HPLC (Nexera X2) with a Kinetex (100 x 3 mm, 2.6 µm; Phenomenex) column. Internal standards for NAD^+ was used to generate standard curves for quantification of NAD^+ concentration.

Cell-free transcription and translation.

In vitro cell-free protein transcription and translation was performed using the PURExpress In vitro Protein Synthesis Kit (New England BioLabs Catalog # E6800S or E6800L). For a total reaction volume of about 25 µL, the reaction was assembled in the following order: 10µL of Solution A, 7.5µL of Solution B, 3µL of RNase inhibitior (40U/µL), and 0.5-1.0 µg of pET30a+ recombinant DNA. Water can be added to bring volume up to 25 µL, but is not necessary. The reaction was incubated at 37°C for 2.5 hours and stopped by placing on ice for a few minutes. Multiple 25 µL reactions can be pooled together to increase protein yield prior to purification of proteins, described below.

Native Protein Purification.

Cell-free synthesized proteins were first purified by Strep Tag affinity methods. 20µL MagStrep (Strep-Tactin) type 3 XT magnetic beads suspension (IBA Lifesciences) was first pre-washed (twice) in binding buffer (50 mM Sodium Phosphate buffer pH ~7.6 – 8.1, 300 mM Sodium Chloride, 0.01% Tween-20), and beads separated using a magnet. Cell-free synthesized proteins (four 25 µL reactions for plant TIRs), were then incubated with the 20µL of MagStrep beads in binding buffer (no more than 500 µL) for 30 min. After 30 min, proteins laden beads were washed three times with binding buffer, and proteins eluted from MagStrep type 3 XT beads with approximately 100µL of 25 mM biotin (Sigma, B4501) for 20-25 min. Biotin eluted proteins were subsequently recaptured via their histidine (His) affinity tag using 10 µL Cobalt (Co^{2+}) Dynabead suspension (pre-washed with binding buffer) for 30 min. cobalt beads laden with proteins were then washed with binding buffer twice, and re-suspended in binding buffer (usually 100 µL) for further NADase enzymatic assays.

In vitro NADase Assay with Purified Protein.

For plant TIR proteins, 20 µL of cobalt beads laden with purified protein were incubated with 2.5 µM NAD^+ (final concentration) and reaction buffer (92.4 mM NaCl and 0.64X PBS), for a total reaction volume of 50 µL. Reactions were carried out at room temperature (25° C) for the indicated amount of time. Reaction was stopped by addition of 50 µL of 1M of perchloric acid ($HClO_4$) and placing the tube on ice for at least 10 min. Neutralization was performed with 16.7 µL 3M K_2CO_3. Samples were placed on ice for 10 min, and then separated by centrifugation. NAD^+ metabolites were quantified by HPLC (see HPLC metabolite measurement above). For LC-MS/MS analysis, the extraction was performed using 90 µL of 50% Methanol in water, and chloroform (see LC-MS metabolite measurement for further details). Reactions using NAD^+ analogs (NaAD, $NADP^+$, NADH, and NADPH) were performed similarly using these analogs as the substrate instead of NAD^+. Metabolites from these reactions were extracted using either the perchloric acid method or 50% methanol in water as described above. Metabolites were analyzed by either HPLC or LC-MS/MS.

SYPRO Ruby Gel Staining.

Purified proteins were resuspended and boiled in Laemmli buffer for 5-10 min and separated on a 4-12% Bis-Tris Plus gel. Gel was then fixed after electrophoresis in 50% Methanol/7% acetic acid for at least 30 min (twice), then incubated overnight in SYPRO Ruby Protein Gel stain (Thermo Fisher). The following day, the gel was washed with 10% methanol/7% acetic acid solution for 30 min, rinsed in distilled water for at least 5 min (twice), and stained proteins were visualized with a UV transilluminator.

Structural Modeling of SARM1.

SARM1 was modeled using Phyre2. The search was done with the 176aa C-terminus of HsSARM1 (aa 549-724) using the *normal* mode against the Protein Data Bank's set of experimentally determined structures.

Catalytic 'E' residue prevalence in TIR-containing proteins across the plant phylogeny.

We investigated the incidence of 'E' residue in TIR-containing proteins across the plant phylogeny using a panel of 106 publicly available plant proteomes (Supplemental

File 1). Multiple isoforms were detected and only the longest coding sequence was retained for downstream analysis. We used hmmscan from the HMMER package to identify TIR-containing proteins (version 3.1b2 http://hmmer.org/; parameters Pfam-A 31.0 --tblout --domtblout --cut_tc;). 8,865 TIR domain sequences, delimited by their envelope coordinates, were extracted using awk, grep, sed, sort and cut command lines. We obtained a multiple sequence alignment (MSA) of all TIR-domains with Ultra-large alignments using Phylogeny-aware Profile (UPP; github commit 53242afa7ee844efb30b7035ae1f86a75b3258e2; defaults;). We then refined the MSA to remove low accuracy sequences (lower than 26% average similarity) and columns with more than 95% gaps using the seq_reformat program of the T-COFFEE suite . The final alignment contained 8,687 TIR domains. Site-specific amino-acid occurrences in the final alignment were computed using in-house bash scripts. Catalytic 'E' incidence in MSA was quantified in R. Alignment visualization as sequence bundles was performed with Alvis.

Identification of putative RPS4 and RRS1 orthologs.

NLRs from all mined proteomes were identified and used in an all-against-all blastp (version 2.6.0; parameters -dbsize 100000000 -evalue 1e-5 -outfmt 6 -num_threads 8). Putative orthologs were identified using orthagogue (orthagogue version 1.0.3; parameters --taxon_index 0 --protein_index 1 --seperator \| --cpu 8 -A -u -S;). Cluster structure of the similarity relationships from previous steps was determined using mcl (version 14-137; parameters --abc -I 1.2 -t 8;). Orthogroups containing the putative orthologs of A. thaliana RPS4 and RRS1 are presented in Supplemental File 2 (*12*).

Statistics.

Figure legends indicate type of statistical test used. Error bars generally represent SEM. For some points where error bars would be shorter than the height of the symbol, Graph Pad Prism software indicates error bars were not drawn.

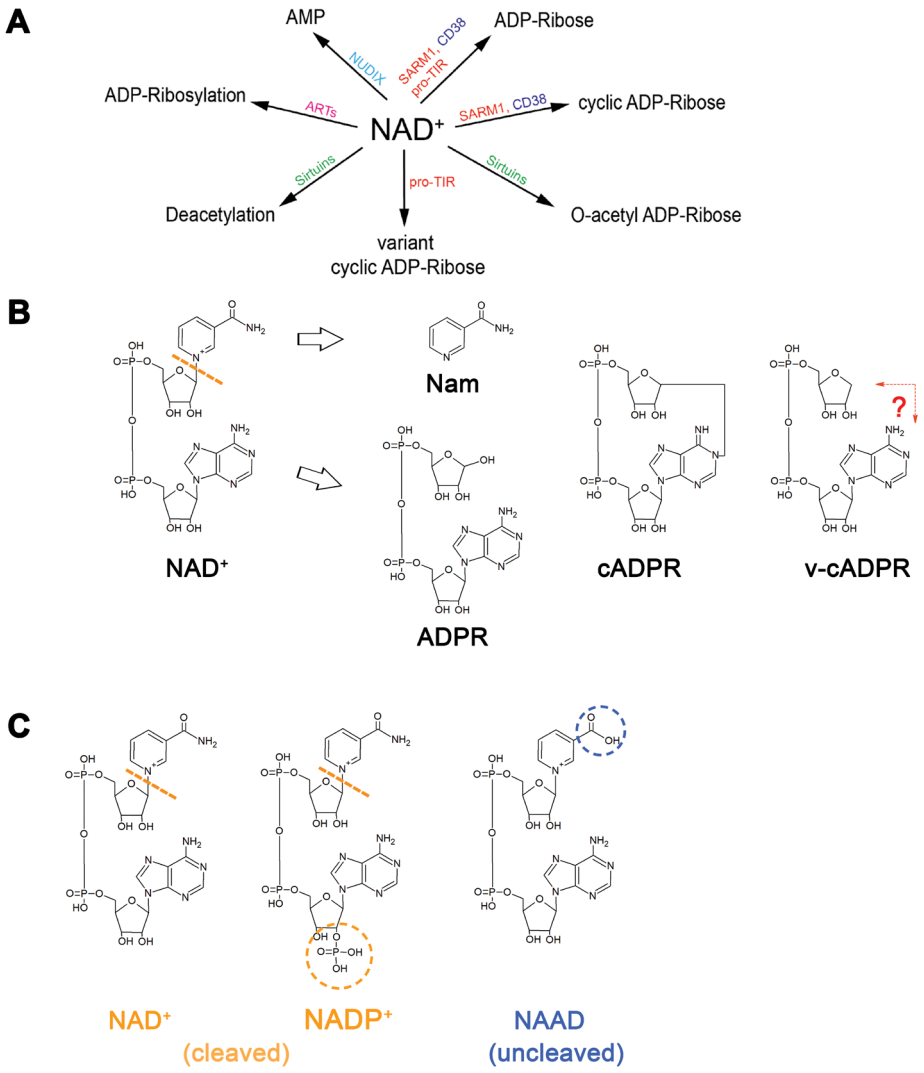

Fig. S1.

NAD$^+$ cleavage products and alternate TIR substrates. (A) NAD$^+$ consuming enzymes. NUDIX – Nudix hydrolases; pro-TIR - prokaryotic TIR; ARTs – ADP-Ribosyltransferase. (B) To varying extents, plant, animal and bacterial TIRs cleave NAD$^+$ into Nam, ADPR, cADPR and v-cADPR. Orange dashed line indicates TIR NAD$^+$ cleavage event. The position of the v-cADPR cyclizing bond is unknown (red arrows), but its parent ion as detected by mass spectrometry is the same as cADPR (see fig S7). (C) NAD$^+$-related molecules tested as alternative substrates in Figure 2L. Cleaved substrates are shown in orange, uncleaved substrates are in blue. The orange dashed circle highlights the NADP$^+$ phosphate group which is compatible with the observed cleavage by RBA1 and BdTIR. Blue dashes indicate carboxyl group that is incompatible with RBA1 and BdTIR cleavage.

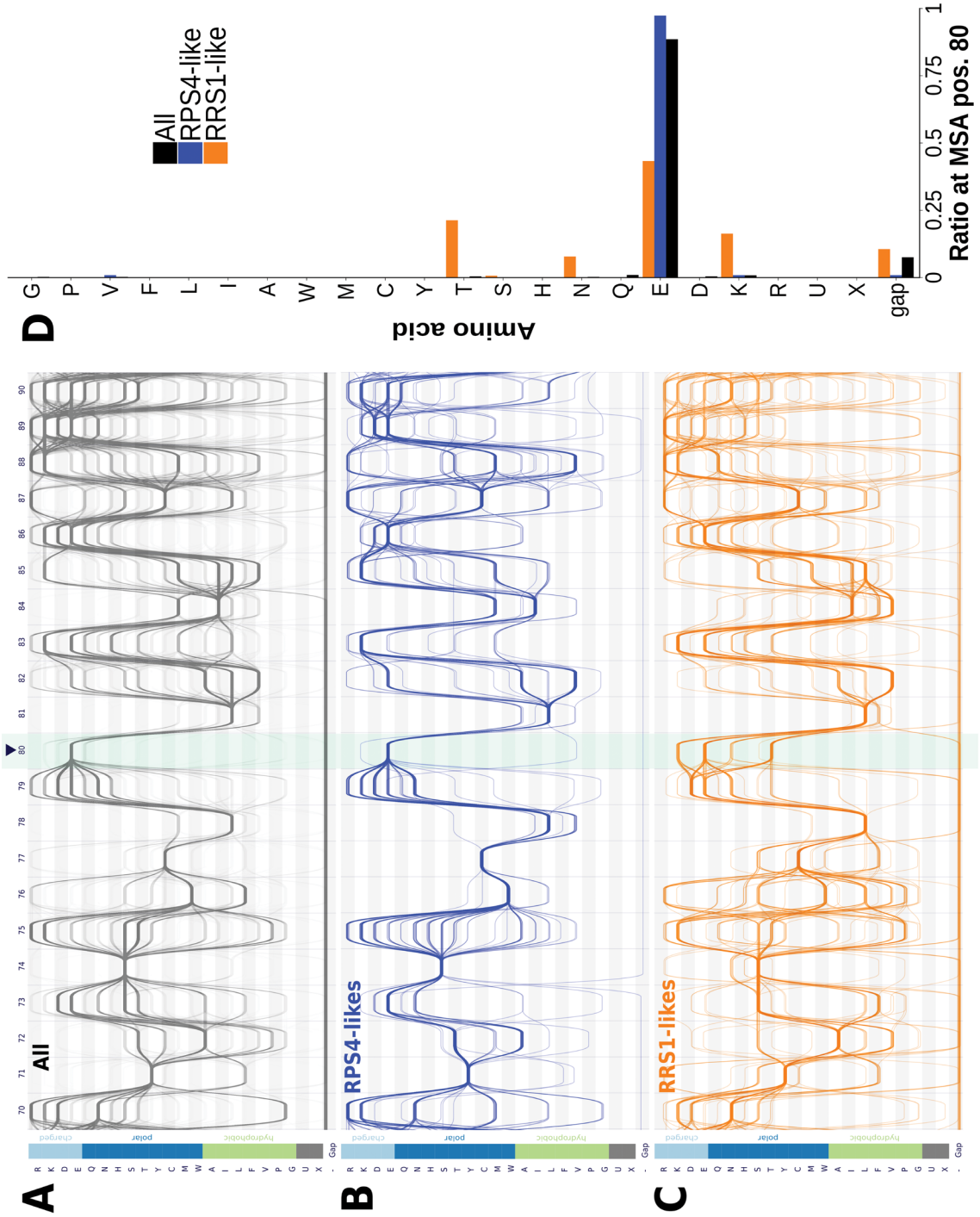

Fig. S2

Catalytic 'E' abundance in TIRs mined from 106 publicly available genomes (related to supplemental file 1 and 2) (A-C) Alvis's sequence bundles visualization of the mined TIR domains. The bundle shows amino acid incidence in three sequence groups in different colours (A) black: All 8,687 mined TIRs ; (B) blue: 113 RPS4-likes; (C) orange: 141 RRS1-likes. Catalytic 'E' residue position is highlighted in light green background. (D) Quantification of amino acids found at position 80 of the MSA.

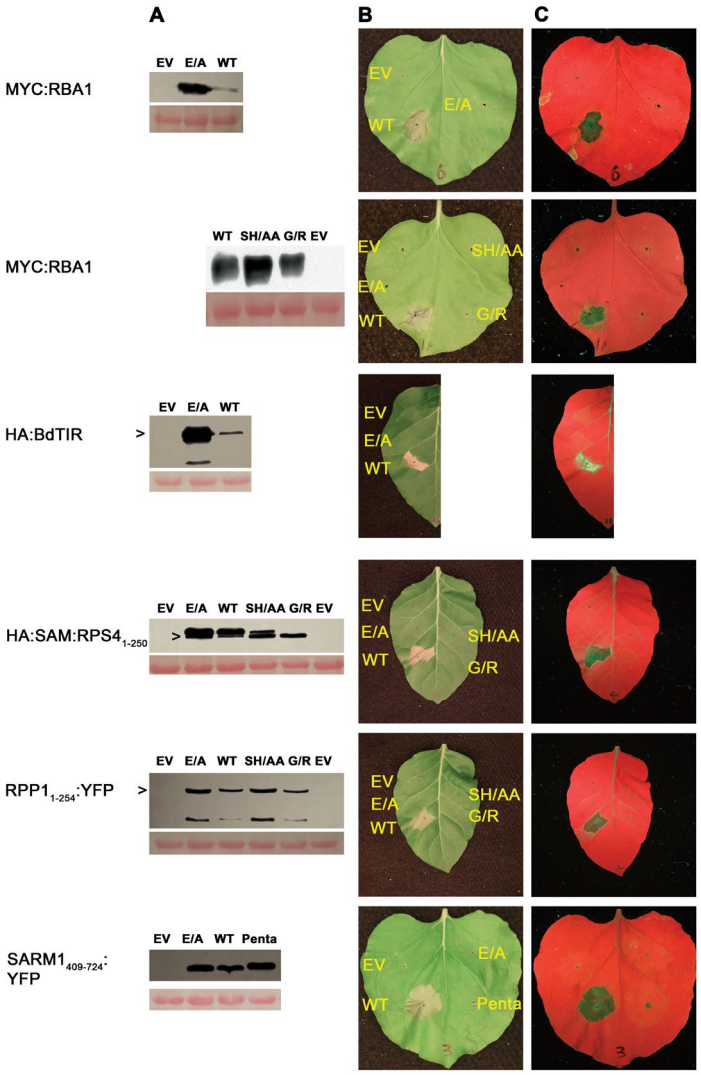

Fig. S3

Phenotypes and protein accumulation of TIR transient expression in *Nicotiana tabacum* or *N. benthamiana*. (A) Protein accumulation of WT and mutant TIR proteins transiently expressed in *Nicotiana* and assayed by western blotting using anti-HA, -MYC or -GFP as appropriate. Ponceau stain indicates protein loading. In the case of multiple bands, carets indicate full-length protein of interest. Protein endpoints and epitope tags: myc:RBA1$_{1-191}$, HA-BdTIR$_{1-224}$, RPP1$_{90-254}$:YFP, HA:SAM-RPS4$_{1-250}$, and HA:HsSAM-TIR$_{409-724}$:YFP (B) Visible light images of autoactive cell death phenotypes triggered by transient TIR overexpression (cell death typically occurred 24 to 48 hours after innoculation). EV is empty vector negative control, E/A is the putative catalytic dead glutamic acid to alanine mutant. SH/AA and G/R are defined or putative self-association mutants. “Penta” is a SARM1 SAM domain self-association mutant (L442R_I461D_L514D_L531D_V533D). RBA1 and SARM1 are expressed in *N. benthamiana*, the others are in *N. tabacum*. (C) UV images of autoactive cell death phenotypes. These images are the source for images in Figure 1.

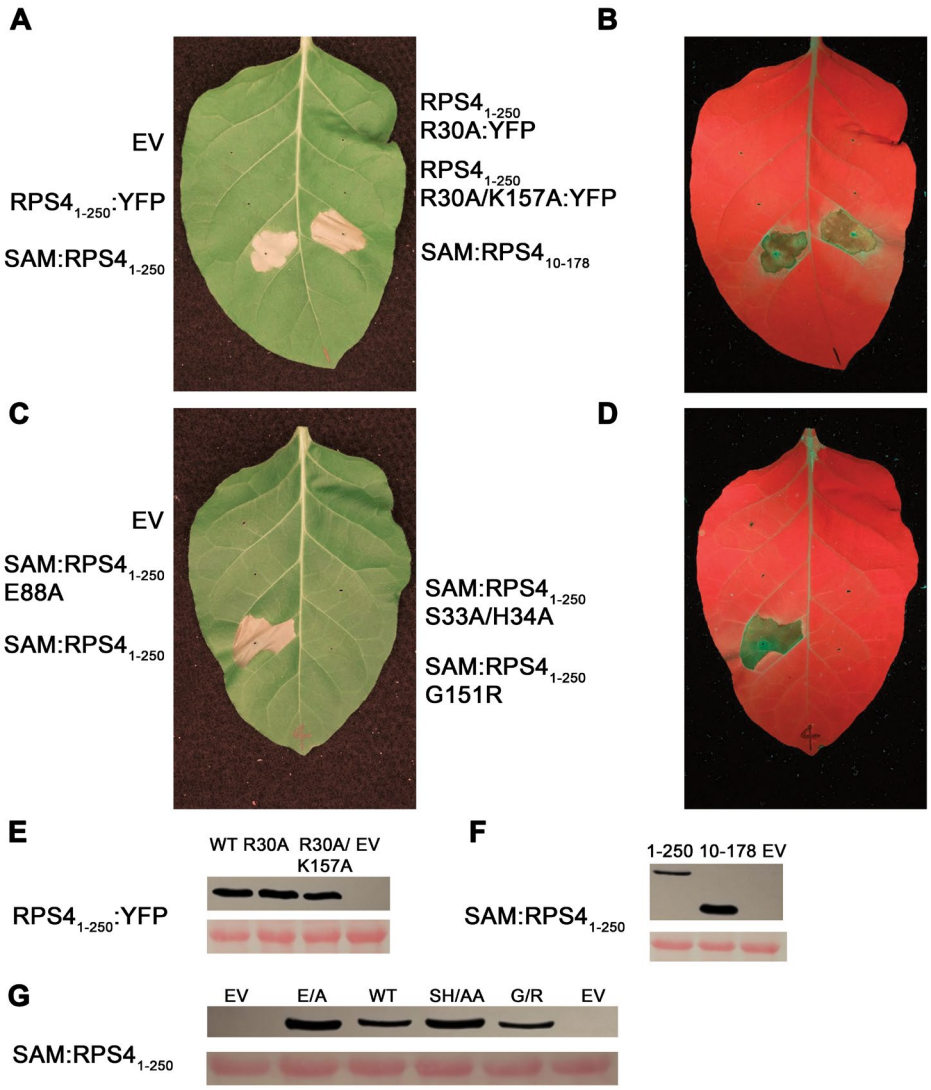

Fig. S4

RPS4 TIR phenotypes. In our hands, RPS4 TIR domain constructs (previously reported as active (13)) did not trigger strong phenotypes in either *Nicotiana tabacum* or *Nicotiana benthamiana*. Since plant TIR domain autoactivity phenotypes have been reported to be correlated with the strength of self-association (15), we generated constructs to enhance self-association of the RPS4-TIR domain using the SAM oligomerization domain of SARM1. (A) Various RPS4 constructs expressed in *N. tabacum*. Cell death is evident only for RPS4 aa1-250 and a "core TIR" aa 10-178 construct fused to the SAM domain of SARM1. Cell death was not evident for RPS4 1-250:YFP or for the same construct containing the enhanced self-association mutation R30A. (B) UV image of the leaf in (A). (C) The autoactive SAM:RPS4 aa1-250 construct requires both the putative catalytic residue E88A and the self-association interfaces defined by S33/H34 and G151 (demonstrated and putative, respectively). (D) UV image of leaf in (C). (E-G) Western blot demonstrating protein accumulation for TIR loss of function mutants. Constructs are blotted with either anti-GFP (RPS4) or anti-HA (SAM:RPS4).

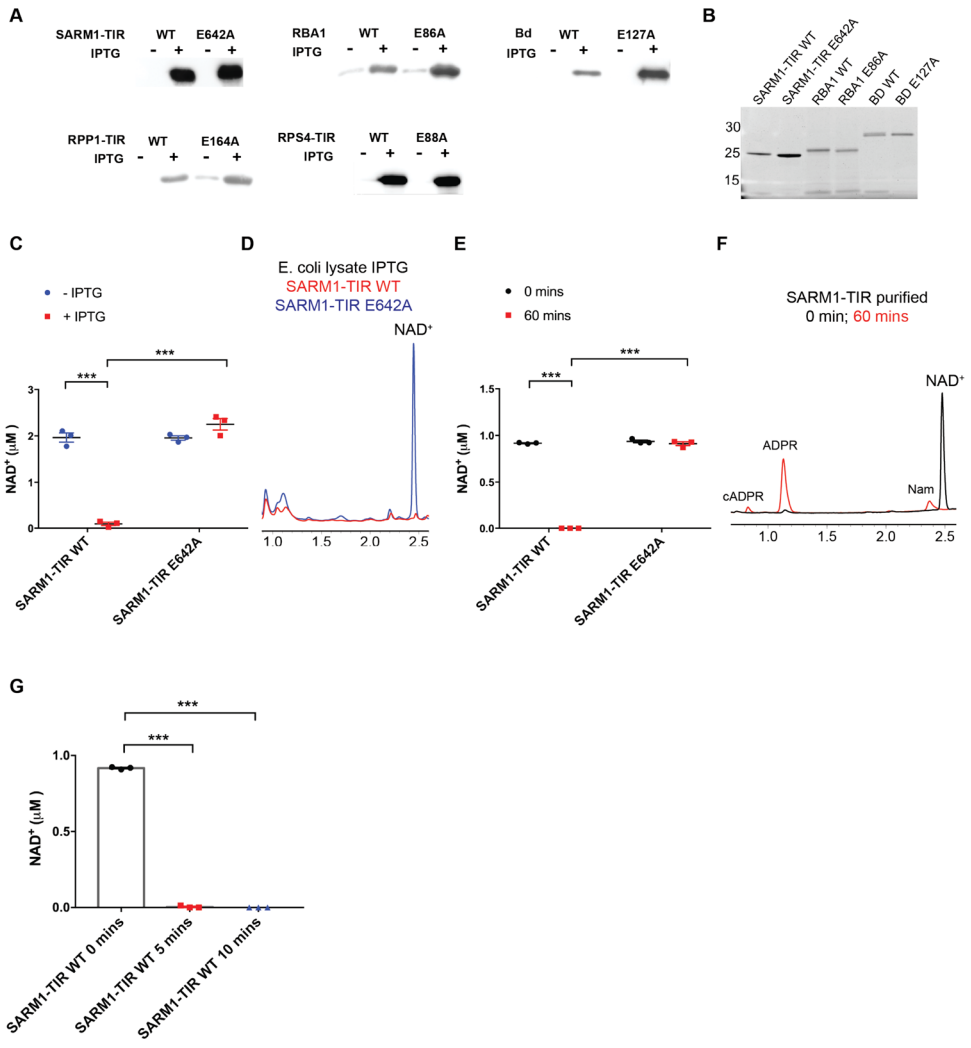

Fig. S5

Protein expression and SARM1-TIR NAD$^+$ cleavage reactions (A) Anti-his tag western blots to confirm protein induction in *E. coli*. Samples correspond to Fig. 2 A to D. (B) SYPRO Ruby Gel stain of WT and E/A mutation of SARM1-TIR, RBA1, and BdTIR to verify protein accumulation for in vitro transcription/translation-based NADase assay in Figure 2I to 2L. (C) SARM1 TIR domain depletes NAD$^+$ after 2 hour IPTG induction in *E. coli* as assayed by HPLC. SARM1 E642A with the putative catalytic glutamic acid mutated to alanine exhibits no depletion. Error bars represent SEM. Asterisks indicate statistical significance in a one-way ANOVA with Tukey's multiple comparison test (*** $p < 0.001$). (D) HPLC chromatogram of E. coli lysate expressing WT SARM1-TIR demonstrates depletion of NAD$^+$. (E) SARM1 TIR protein generated by in vitro transcription-translation depletes NAD$^+$ after 60min. Putative catalytic glutamic acid to alanine mutant does not deplete NAD$^+$. Statistics are performed as in (C). (F) HPLC traces corresponding to (E) indicate that purified SARM1-TIR generates Nam, ADPR and cADPR when incubated with NAD$^+$, but not v-cADPR. (G) In vitro assays (as in E) showing that SARM1 TIR rapidly depletes NAD$^+$. The 0 minute timepoint data are shared in (E) and (G). Statistics are performed as in (C).

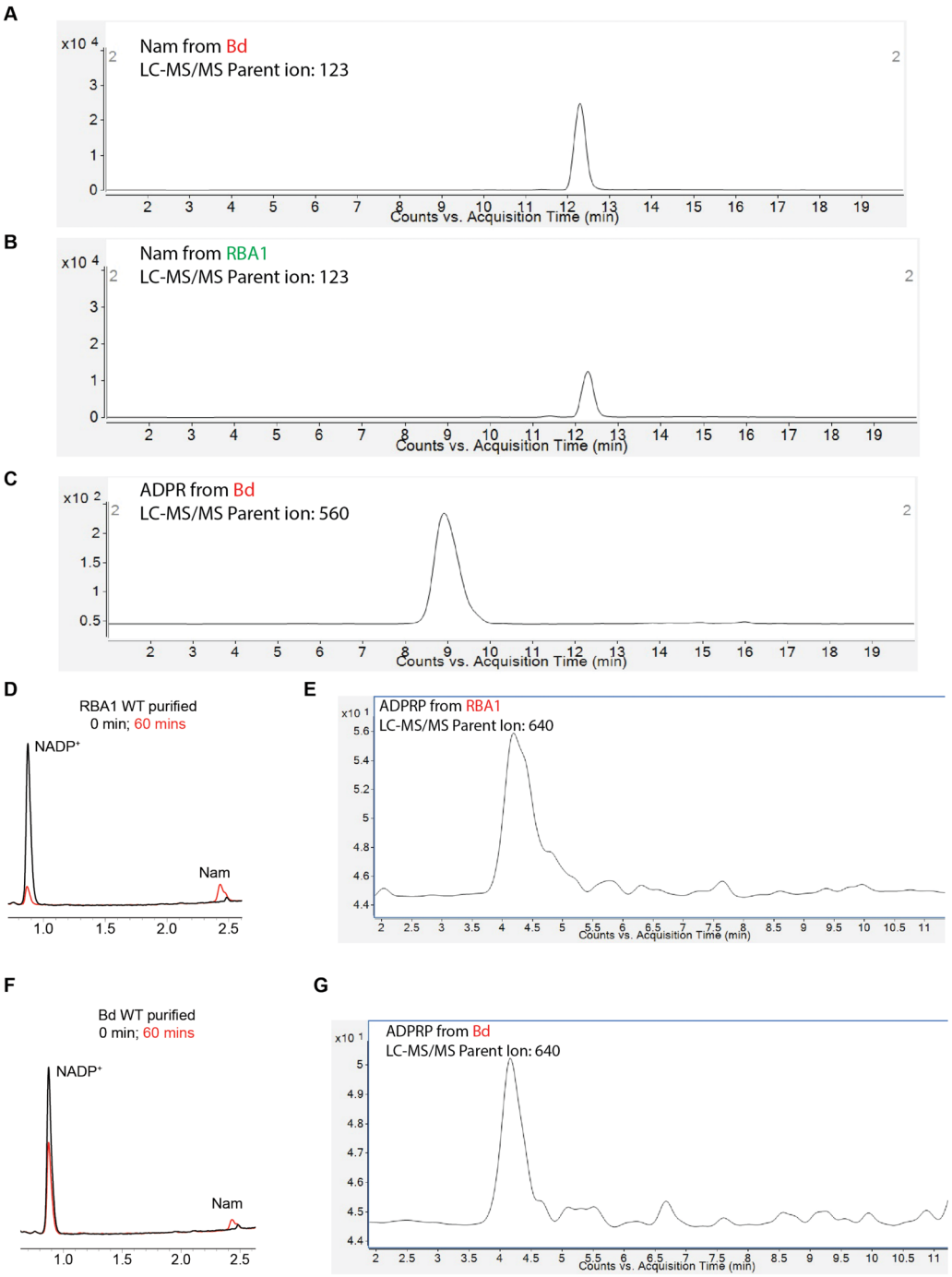

Fig. S6

LC-MS/MS and HPLC chromatograms of TIR in vitro assay products. (A-C) LC-MS/MS profiles identifying Nam (BdTIR and RBA1) and ADPR (BdTIR) as in vitro NAD^+ cleavage products of in vitro transcription/translation produced TIR proteins. (D-E) In vitro transcription/translation produced RBA1 cleaves $NADP^+$ into Nam and ADPRP. (F-G) In vitro transcription/translation produced BdTIR cleaves $NADP^+$ into Nam and ADPRP.

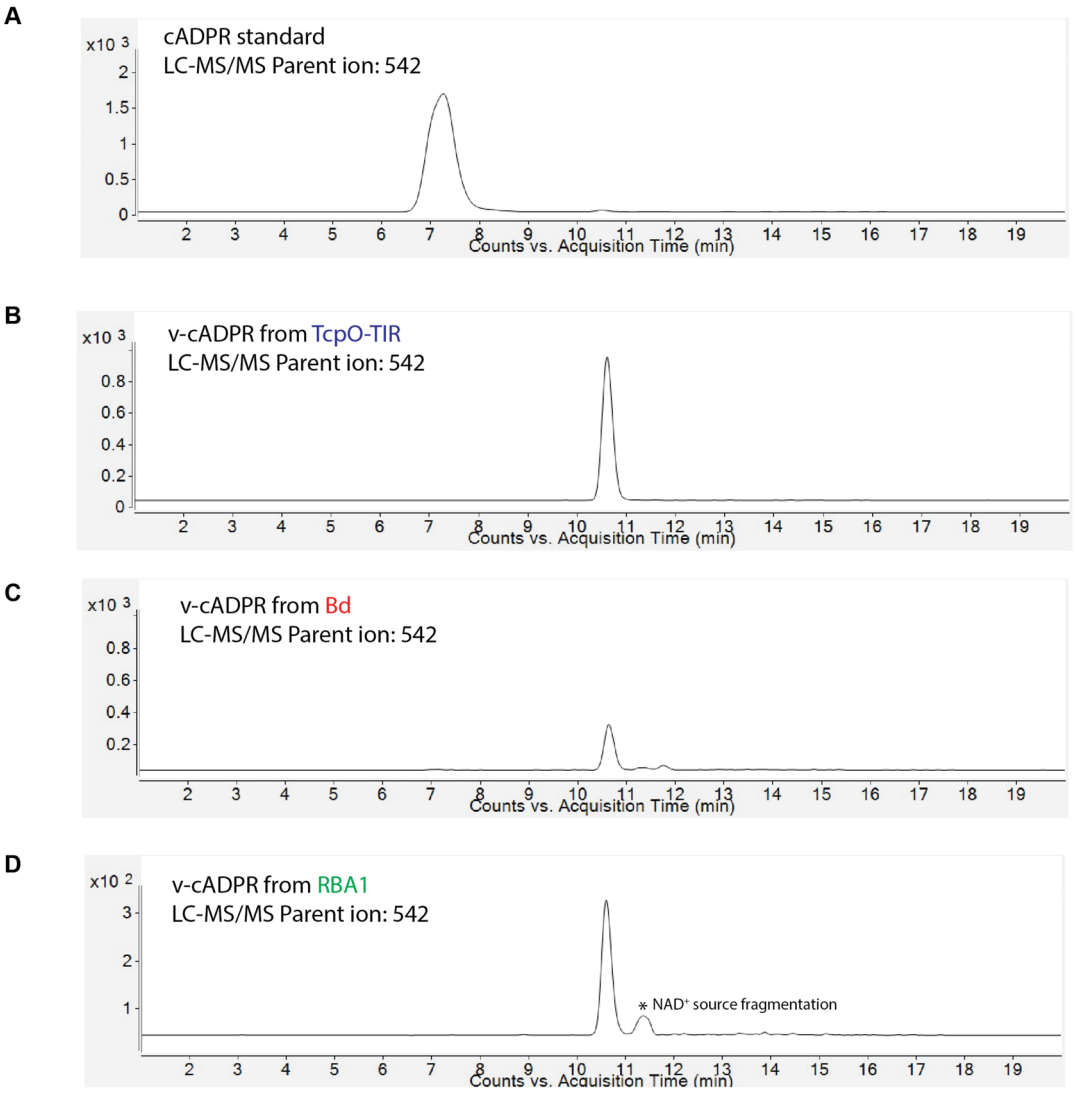

Fig. S7

Comparison of v-cADPR and cADPR. (A-D) Comparison of v-cADPR identified as a plant TIR NADase product, v-cADPR from archeal TcpO TIR domain, and commercially available cADPR. v-cADPR and cADPR share the same parent ion, but display different retention times suggestive of alternate cyclization.

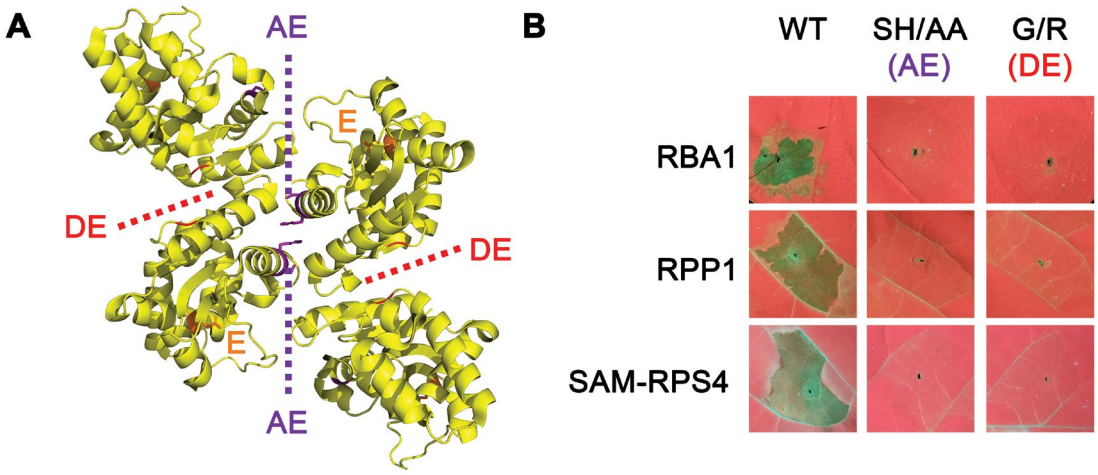

Fig. S8

Plant TIR enzymatic activity and cell death induction requires self-association. (A) RPP1 structure (PDB 5TEB) indicating self-association interfaces. The AE interface is indicated by purple dashes and purple amino acids S108 H109. The DE interface is indicated by red dashes and the red amino acid G229. The putative catalytic glutamic acid is colored in orange. (B) Autoactivity triggered by RBA1, RPP1 and SAM1-RPS4 (constructs as described in Fig 1C) in Nicotiana spp. is dependent on by AE and DE interfaces as defined by loss of function mutations (SH/AA or G/R). RPP1 and SAM-RPS4 images are from the same experiment presented in Figure 1.

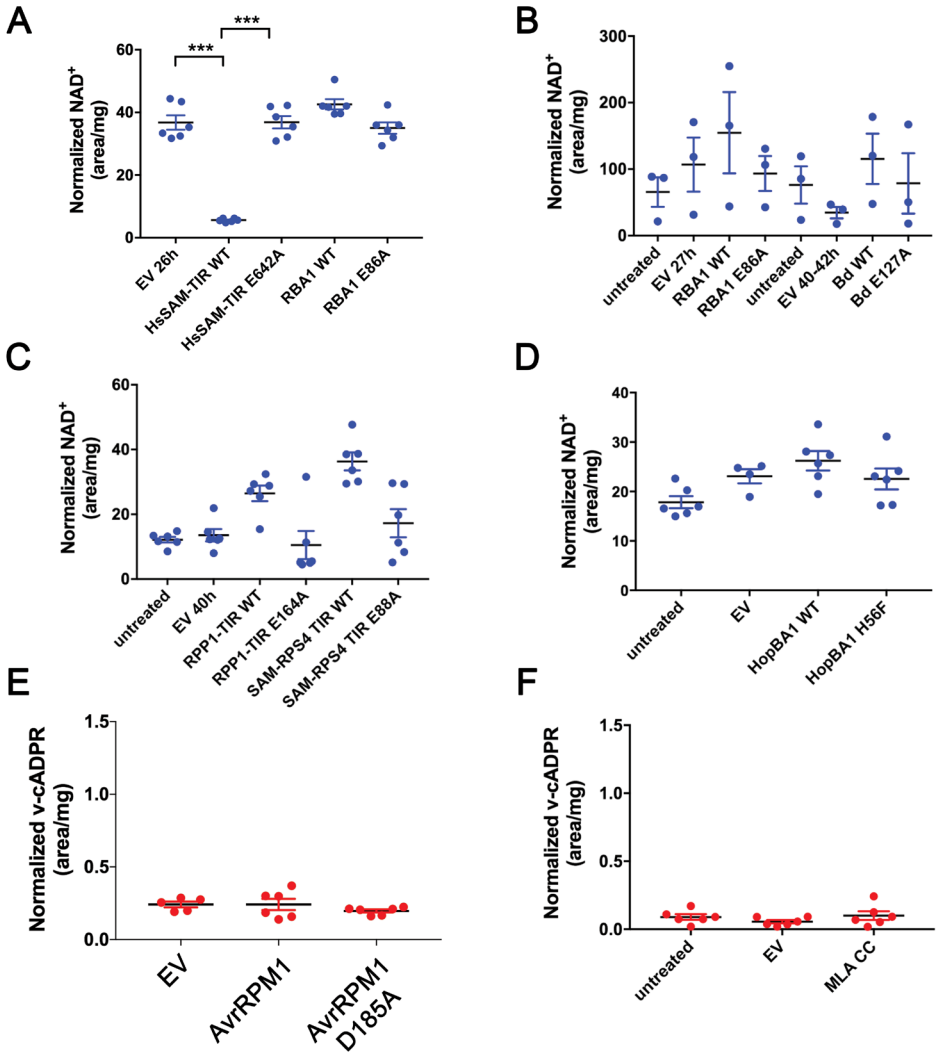

Fig. S9

In planta NAD$^+$ depletion assays; Cell death triggered by the non-TIR NLR RPM1 or the CC domain of MLA10 is insufficient to trigger v-cADPR accumulation. (A) Transient expression of HsSAM-TIR in *N. benthamiana* reduces NAD$^+$ accumulation relative to the putative catalytic mutant HsSAM-TIR E642A. Expression of RBA1 does not deplete NAD$^+$. Error bars represent SEM. Asterisks indicate statistical significance in a one-way ANOVA with Tukey's multiple comparison test (*** $p < 0.001$). (B) Plant TIR-only proteins do not measurably deplete NAD$^+$ when transiently expressed in *N. benthamiana*. (C) Plant TIR domains from TNL immune receptors do not measurably deplete NAD$^+$ when expressed in *N. benthamiana*. (D) Delivery of HopBA1 (to trigger TIR-only RBA1) by *P. fluorescens* does not result in measurable NAD$^+$ depletion in Arabidopsis (Ag-0). (E) Bacterial delivery of AvrRpm1 (pathogen effector recognized by the CNL immune receptor RPM1) into Arabidopsis accession Col-0 did not result in accumulation of v-cADPR in excess of empty vector (EV) or the loss of function mutant AvrRpm1 D185A. (F) Overexpression of MLA10 aa1-160 CC domain in *N. benthamiana* does not result in accumulation of v-cADPR.

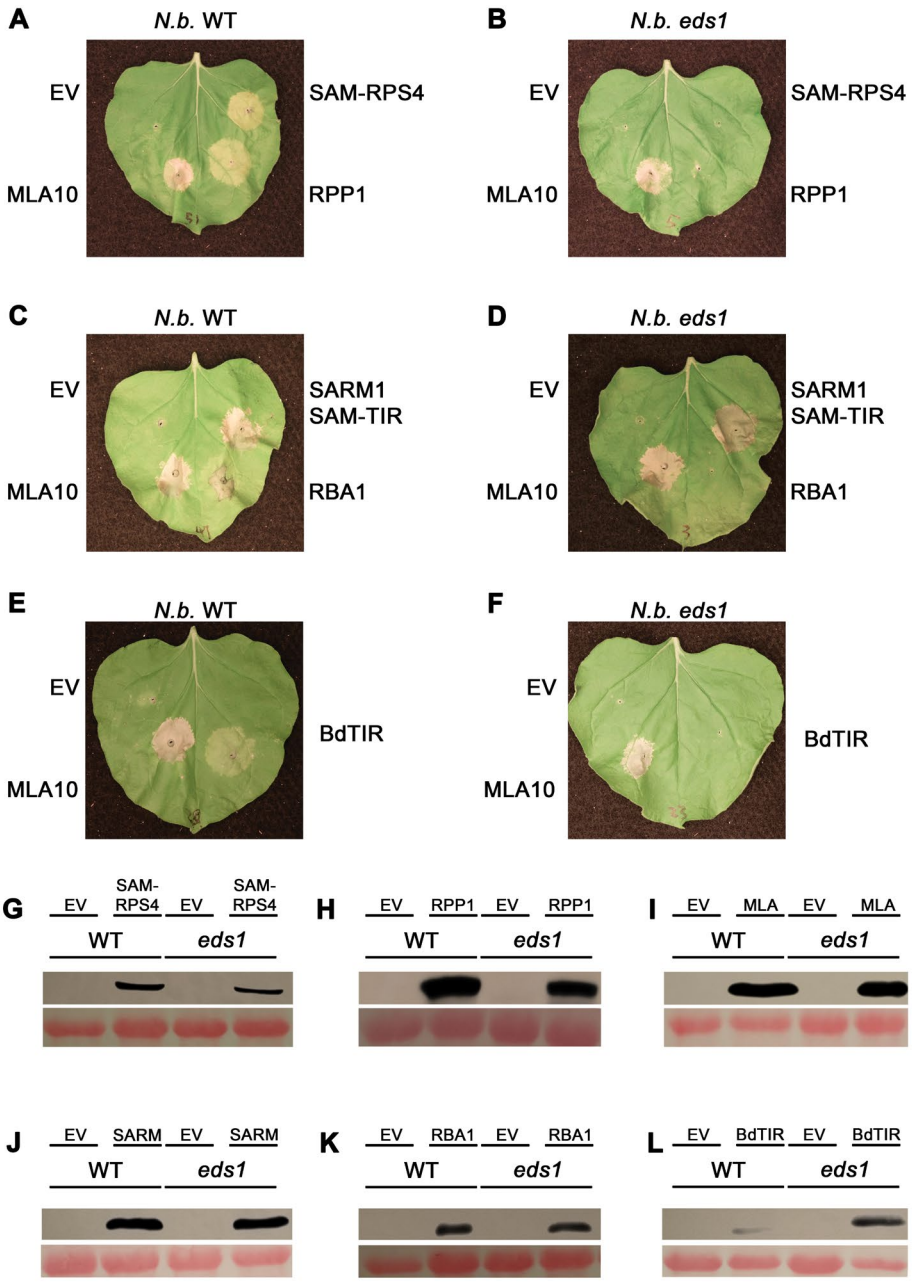

Fig. S10

Plant TIR autoactivity is EDS1-dependent. (A-F) Transient expression of plant TIRs in either WT or *eds1-2* mutant *Nicotiana benthamiana*. In all cases, plant TIR autoactivity is *EDS1*-dependent. An autoactive SAM-TIR truncation of Human SARM1 (aa 409-724) retains autoactivity in *eds1*. EV is an empty vector negative control. MLA10 (CC domain; aa1-160) is used here as a known EDS1-independent positive control. TIR constructs are as described in Fig 1 and fig S3. (G-L) Western blots to confirm protein accumulation of non-active TIRs in *eds1* plants. Antibodies used were specific to the various epitope tags (HA:SAM-RPS4, RPP1:YFP, MLA:MYC, SARM1 SAM-TIR:YFP, MYC:RBA1, and HA:BdTIR). Ponceau stain indicates equal loading.

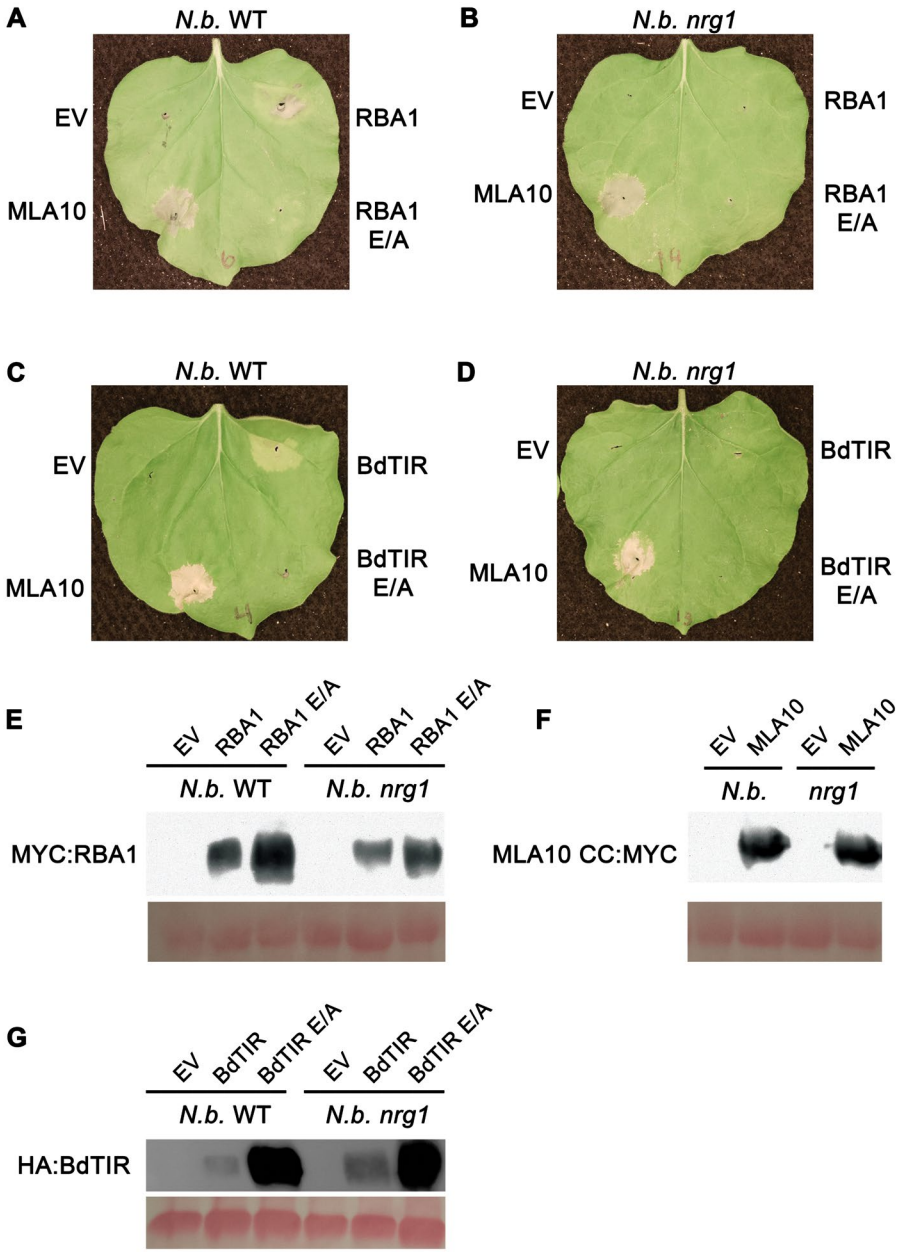

Fig. S11

RBA1 and BdTIR cell death requires NRG1. RBA1 autoactive cell death in *N. benthamiana* (A) is lost in an *nrg1* mutant (B). EV is an empty vector negative control. MLA10 (CC domain, aa1-160) is a non-TIR positive control for autoactive cell death in *nrg1*. BdTIR autoactive cell death in *N. benthamiana* (C) is lost in an *nrg1* mutant (D). (E and F) anti-MYC western blot demonstrates RBA1 and MLA10 protein accumulation in *nrg1* plants. (G) anti-HA western blot demonstrates BdTIR protein accumulation in *nrg1* plants.

Template	Confidence	%i.d.	Template Information	Source
c3oziB	99.9	18	Crystal structure of the tir domain from the flax protein L6	Plant
c4lzpA	99.9	21	Structure of the tir domain of the immunosuppressor BtpA	Bacteria
c5tebC	99.9	17	Crystal structure of the tir domain from RPP1	Plant
c4lzpB	99.9	21	Structure of the tir domain of the immunosuppressor BtpA	Bacteria
c5ku7B	99.9	21	Crystal structure of the tir domain from RPV1	Plant
c4c6rB	99.9	17	Crystal structure of the tir domain from RPS4	Plant
c3h16A	99.9	22	Crystal structure of a bacteria tir domain, PdTIR	Bacteria
c4w8hA	99.9	17	Crystal structure of the tir domain of the toll-related receptor trr-22	Animal
d1fyva	99.9	14	Toll/interleukin receptor TIR domain TLR1	Animal
c2j67B	99.8	17	The tir domain of human toll-like receptor 10	Animal

Table S1.

Summary of top ten results returned from HsSARM1 Phyre2 search.

Gene	Local region of E	Gene type	Notes
AT1G72850	ISVLCLN**Q**LEKIVNS	TIR-NB	head to head with neighboring TIR
AT1G72870	SSVLCLD**V**LAKIIER	TIR-NB	head to head with neighboring TIR
AT4G12020	----VPS**N**LLNILEH	WRKY-TIR-NB-LRR-PK	*RPS4/RRS1*-like (Narusaka, 2009)
AT4G16930	---------------	TIR	truncated
AT4G19500	SSRQSLD**H**LVAVMEH	TIR-NB-**TIR**-NB-LRR	in second TIR
AT4G36140	SSTSCLD**M**LVRVFQC	TIR-NB-**TIR**-NB-LRR	*RPS4/RRS1*-like (Narusaka, 2009); in second TIR
AT5G17890	YDPWFPK**F**LKVIQGW	TIR-NB-LRR-LIM	*RPS4/RRS1*-like (Narusaka, 2009)
AT5G38850	EHLGTIR**D**RLHDQKV	TIR-TIR-NB-LRR	in second TIR
AT5G45050	--TVSLD**K**LVKVLDC	TIR-NB-LRR-WRKY	*RPS4/RRS1*-like (Narusaka, 2009)
AT5G45090	D----FN**D**LLKNNES	TIR-PP	
AT5G45210	LSKQCLD**T**LVEFLER	TIR-NB-LRR	*RPS4/RRS1*-like (Narusaka, 2009)
AT5G45220	ESKWCLM**K**LVDINKC	TIR-TIR	
AT5G45240	SSVLCLE**N**LELC--C	TIR-NB-LRR	head to head with neighboring TIR
AT5G45260	PSEVWLD**K**FAKVLEC	TIR-NB-LRR-WRKY	*RRS1*; *RPS4/RRS1*-like (Narusaka, 2009)
AT5G48780	SSPLCLD**S**LLKILKF	TIR-NB	head to head with neighboring TIR

Table S2.

Arabidopsis thaliana (Col-0) TIR proteins with non-conserved glutamic acid are typically non-canonical.

Gene	Context	Mutation	Approach	Reference
RPS4	TIR domain	E88A	Site-directed	Swiderski, et al (2009)
RPS4	TNL	E88K	EMS screen	Sohn, et al (2014)
RPP1	TIR domain	E158A	Site-directed	Krasileva, et al (2010)
SOC3	TNL	E86K	EMS screen	Tong, et al (2017)

Table S3.

Summary of published plant TIRs with a mutated SARM1-like putative catalytic glutamate residue.

Additional Data S1 (separate file)

List of plant genomes scanned for conservation of putative catalytic glutamic acid residue (related to fig. S2).

Additional Data S2 (separate file)

List of Arabidopsis RRS1-like genes (related to fig. S2).

Additional Data S3 (separate file)

R script used to generate fig. S2 depicting conservation of putative catalytic glutamic acid across plant TIR domains.

References and Notes

1. J. D. G. Jones, J. L. Dangl, The plant immune system. *Nature* **444**, 323–329 (2006). doi:10.1038/nature05286 Medline

2. J. D. G. Jones, R. E. Vance, J. L. Dangl, Intracellular innate immune surveillance devices in plants and animals. *Science* **354**, aaf6395 (2016). doi:10.1126/science.aaf6395 Medline

3. X. Zhang, P. N. Dodds, M. Bernoux, What Do We Know About NOD-Like Receptors in Plant Immunity? *Annu. Rev. Phytopathol.* **55**, 205–229 (2017). doi:10.1146/annurev-phyto-080516-035250 Medline

4. J. Gerdts, E. J. Brace, Y. Sasaki, A. DiAntonio, J. Milbrandt, SARM1 activation triggers axon degeneration locally via NAD^+ destruction. *Science* **348**, 453–457 (2015). doi:10.1126/science.1258366 Medline

5. J. Gerdts, D. W. Summers, Y. Sasaki, A. DiAntonio, J. Milbrandt, Sarm1-mediated axon degeneration requires both SAM and TIR interactions. *J. Neurosci.* **33**, 13569–13580 (2013). doi:10.1523/JNEUROSCI.1197-13.2013 Medline

6. K. Essuman, D. W. Summers, Y. Sasaki, X. Mao, A. DiAntonio, J. Milbrandt, The SARM1 Toll/Interleukin-1 Receptor Domain Possesses Intrinsic NAD^+ Cleavage Activity that Promotes Pathological Axonal Degeneration. *Neuron* **93**, 1334–1343.e5 (2017). doi:10.1016/j.neuron.2017.02.022 Medline

7. K. Essuman, D. W. Summers, Y. Sasaki, X. Mao, A. K. Y. Yim, A. DiAntonio, J. Milbrandt, TIR Domain Proteins Are an Ancient Family of NAD^+-Consuming Enzymes. *Curr. Biol.* **28**, 421–430.e4 (2018). doi:10.1016/j.cub.2017.12.024 Medline

8. D. Pajuelo, N. Gonzalez-Juarbe, U. Tak, J. Sun, C. J. Orihuela, M. Niederweis, NAD^+ Depletion Triggers Macrophage Necroptosis, a Cell Death Pathway Exploited by Mycobacterium tuberculosis. *Cell Rep.* **24**, 429–440 (2018). doi:10.1016/j.celrep.2018.06.042 Medline

9. T. Shidore, C. D. Broeckling, J. S. Kirkwood, J. J. Long, J. Miao, B. Zhao, J. E. Leach, L. R. Triplett, The effector AvrRxo1 phosphorylates NAD in planta. *PLOS Pathog.* **13**, e1006442 (2017). doi:10.1371/journal.ppat.1006442 Medline

10. S. Doron, S. Melamed, G. Ofir, A. Leavitt, A. Lopatina, M. Keren, G. Amitai, R. Sorek, Systematic discovery of antiphage defense systems in the microbial pangenome. *Science* **359**, eaar4120 (2018). doi:10.1126/science.aar4120 Medline

11. J. Y. Tang, N. P. Bullen, S. Ahmad, J. C. Whitney, Diverse NADase effector families mediate interbacterial antagonism via the type VI secretion system. *J. Biol. Chem.* **293**, 1504–1514 (2018). doi:10.1074/jbc.RA117.000178 Medline

12. M. Narusaka, K. Shirasu, Y. Noutoshi, Y. Kubo, T. Shiraishi, M. Iwabuchi, Y. Narusaka, RRS1 and RPS4 provide a dual Resistance-gene system against fungal and bacterial pathogens. *Plant J.* **60**, 218–226 (2009). doi:10.1111/j.1365-313X.2009.03949.x Medline

13. S. J. Williams, K. H. Sohn, L. Wan, M. Bernoux, P. F. Sarris, C. Segonzac, T. Ve, Y. Ma, S. B. Saucet, D. J. Ericsson, L. W. Casey, T. Lonhienne, D. J. Winzor, X. Zhang, A. Coerdt, J. E. Parker, P. N. Dodds, B. Kobe, J. D. G. Jones, Structural basis for assembly and

function of a heterodimeric plant immune receptor. *Science* **344**, 299–303 (2014). doi:10.1126/science.1247357 Medline

14. M. T. Nishimura, R. G. Anderson, K. A. Cherkis, T. F. Law, Q. L. Liu, M. Machius, Z. L. Nimchuk, L. Yang, E.-H. Chung, F. El Kasmi, M. Hyunh, E. Osborne Nishimura, J. E. Sondek, J. L. Dangl, TIR-only protein RBA1 recognizes a pathogen effector to regulate cell death in *Arabidopsis*. *Proc. Natl. Acad. Sci. U.S.A.* **114**, E2053–E2062 (2017). doi:10.1073/pnas.1620973114 Medline

15. K. J. Schreiber, A. Bentham, S. J. Williams, B. Kobe, B. J. Staskawicz, Multiple Domain Associations within the Arabidopsis Immune Receptor RPP1 Regulate the Activation of Programmed Cell Death. *PLOS Pathog.* **12**, e1005769 (2016). doi:10.1371/journal.ppat.1005769 Medline

16. Z. Q. Shao, J.-Y. Xue, P. Wu, Y.-M. Zhang, Y. Wu, Y.-Y. Hang, B. Wang, J.-Q. Chen, Large-Scale Analyses of Angiosperm Nucleotide-Binding Site-Leucine-Rich Repeat Genes Reveal Three Anciently Diverged Classes with Distinct Evolutionary Patterns. *Plant Physiol.* **170**, 2095–2109 (2016). doi:10.1104/pp.15.01487 Medline

17. R. Fliegert, A. Gasser, A. H. Guse, Regulation of calcium signalling by adenine-based second messengers. *Biochem. Soc. Trans.* **35**, 109–114 (2007). doi:10.1042/BST0350109 Medline

18. Y. Wu, J. Kuzma, E. Maréchal, R. Graeff, H. C. Lee, R. Foster, N. H. Chua, Abscisic acid signaling through cyclic ADP-ribose in plants. *Science* **278**, 2126–2130 (1997). doi:10.1126/science.278.5346.2126 Medline

19. M. Grant, I. Brown, S. Adams, M. Knight, A. Ainslie, J. Mansfield, The RPM1 plant disease resistance gene facilitates a rapid and sustained increase in cytosolic calcium that is necessary for the oxidative burst and hypersensitive cell death. *Plant J.* **23**, 441–450 (2000). doi:10.1046/j.1365-313x.2000.00804.x Medline

20. N. Aarts, M. Metz, E. Holub, B. J. Staskawicz, M. J. Daniels, J. E. Parker, Different requirements for EDS1 and NDR1 by disease resistance genes define at least two R gene-mediated signaling pathways in Arabidopsis. *Proc. Natl. Acad. Sci. U.S.A.* **95**, 10306–10311 (1998). doi:10.1073/pnas.95.17.10306 Medline

21. S. Wagner, J. Stuttmann, S. Rietz, R. Guerois, E. Brunstein, J. Bautor, K. Niefind, J. E. Parker, Structural basis for signaling by exclusive EDS1 heteromeric complexes with SAG101 or PAD4 in plant innate immunity. *Cell Host Microbe* **14**, 619–630 (2013). doi:10.1016/j.chom.2013.11.006 Medline

22. S. U. Huh, V. Cevik, P. Ding, Z. Duxbury, Y. Ma, L. Tomlinson, P. F. Sarris, J. D. G. Jones, Protein-protein interactions in the RPS4/RRS1 immune receptor complex. *PLOS Pathog.* **13**, e1006376 (2017). doi:10.1371/journal.ppat.1006376 Medline

23. T. Qi, K. Seong, D. P. T. Thomazella, J. R. Kim, J. Pham, E. Seo, M.-J. Cho, A. Schultink, B. J. Staskawicz, NRG1 functions downstream of EDS1 to regulate TIR-NLR-mediated plant immunity in *Nicotiana benthamiana*. *Proc. Natl. Acad. Sci. U.S.A.* **115**, E10979–E10987 (2018). doi:10.1073/pnas.1814856115 Medline

24. T. G. Demarest, M. Babbar, M. N. Okur, X. Dan, D. L. Croteau, N. B. Fakouri, M. P. Mattson, V. A. Bohr, NAD+ Metabolism in Aging and Cancer. *Annu. Rev. Cancer Biol.* **3**, 105–130 (2019). doi:10.1146/annurev-cancerbio-030518-055905